THEORETICAL & APPLIED MECHANICS LETTERS **4**, 021006 (2014)

A novel 3D geometrical reconstruction method for aluminum foams and FEM modeling of the material response

Xiaolei Zhu,[1, a)] Shigang Ai,[2, b)] Xiaofeng Lu,[3, c)] Lingxue Zhu,[4, d)] Bin Liu[1, e)]
[1)]*AML, Department of Engineering Mechanics, Tsinghua University, Beijing 100084, China*
[2)]*State Key Laboratory of Turbulence and Complex System, College of Engineering, Peking University, Beijing 100871, China*
[3)]*Department of Mechanical Engineering, Nanjing University of Technology, Nanjing 211816, China*
[4)]*Department of Mathematics, Jinling Institute of Technology, Nanjing 211169, China*

(Received 7 November 2013; revised 7 December 2013; accepted 2 January 2014)

Abstract A novel method for modeling cellular materials is proposed based on MATLAB image processing and synchrotron X-ray computed tomography scanning to obtain an accurate calculation result of aluminum foam based on finite element model. The maximum entropy algorithm is employed to obtain the binarization image, and the median filtering algorithm is used to reduce the noise after binarization. The external contour and internal pores boundary is extracted by the "edge" function in MATLAB, and the geometrical model is reconstructed. A two-step mesh algorithm is adopted to mesh the reconstructed geometrical model. Accordingly, the finite element model of aluminum foam is established by the proposed method based on reconstruction geometrical model. The compression behavior of aluminum foam is obtained at 25°C, 100°C, 200°C by ABAQUS, and good agreements with experiments are achieved by applying the present reconstruction algorithm and modeling method.

 [doi:10.1063/2.1402106]

Keywords aluminum foam, reconstruction geometrical, compression, X-ray computed tomography

Metal foams have become a new family of materials exhibiting well physical and mechanical properties. This makes them attractive in a lot of engineering applications like energy absorption, lightweight structures, thermal and acoustic management, and lots of studies have been performed out on this type of materials.[1–5]

As in process of fabrication, there would be a plenty of defects in the material, such as uneven pore structure, poor reproducibility in both the preparation process and the measurement result. Therefore, a more accurate numerical prediction of the mechanical and thermal properties of these materials depends on an accurate geometrical model which could reflect the true features of the materials. Many scholars have made efforts to establish a relationship between microstructure and foam materials' properties. As the microstructure of foam materials are mostly 3D which mainly

[a)]Email: zhuxiaolei856028@126.com.
[b)]Email: sgai@pku.edu.cn.
[c)]Email: xflu@njut.edu.cn.
[d)]Corresponding author. Email: lxzhu_jlu@126.com.
[e)]Corresponding author. Email: liubin@tsinghua.edu.cn.

affect the mechanical behavior of cellular materials, it is difficult to construct a relationship between the structure and properties in foam materials due to the complexity of the 3D structure of foam materials. Finite element model (FEM) was usually intended to reveal the relationship between the internal microstructure and its mechanical properties by establishing various simplified models, for example, the elastic spider network model,[6] cube structure model,[7] Gibson–Ashby model,[8] tetrahedral pillar structure model,[9] cubo-octahedron model of the open-cell foam material,[10] and the Voronoi model of open-cell foam material developed in recent years,[11] of which the Voronoi model has been widely used. The Voronoi model is established based on the regular cell structure by using a regular distribution of seed by van den Burg et al.[11] Three special seed distributions (body-centered cubic, face-centered cubic, and nearly hexagonal) were selected to establish each Voronoi open-cell foam metal structure model. The Voronoi model was similar to the real foam foaming preparation process in the generation of internal cell structure, and therefore can be used to simulate the internal structure of foam materials. However, there will be a great error in the calculation results caused by these simplified models when there is a hole through the matrix or the thickness of the pores wall is uneven.

Some other scholars reconstructed the geometrical model by dealing with synchrotron X-ray computed tomography (μCT) scanning images of real aluminum foam.[12–16] Constructing such FE models that can supply a fairly accurate description of cellular materials' actual geometry is critical to get a high-quality prediction of porous materials response. The traditional reconstruction approach was to import these coordinates of pixels into reverse engineering software (such as Geomagic Studio, ImageJ, PRO/E) making geometric model by lofting, surface fitting, and some other ways, and then to generate the STereo Lithography (STL) file. The geometric model was established by importing the STL file into 3D computer-aided drawing (CAD) software, and then importing the geometric model into FE analysis software to establish an FEM for foam materials.[17–21] However, due to numerous holes inside the foam materials and random distribution, there is a great difference between the actual model and the reconstructed geometrical model using reverse engineering, which makes the calculation results unsatisfied.

In this paper, a novel method for modeling cellular materials was proposed based on MATLAB image processing and μCT scanning. This method was used to reconstruct the aluminum foam and establish an FEM with 14 mm diameter and 8 mm height. The compression behavior of aluminum based on the reconstructed geometrical model is calculated at 25°C, 100°C, 200°C, respectively, and the results were compared with experimental results.

In the process of scanning the aluminum foam by using μCT, the external environment, devices, and the distortion of the image format in conversion process would lead to blurred images of edges. In order to extract useful information from the image, it must be pre-processed. The effective information will be highlighted, and the noise will be reduced. The MATLAB is used to process μCT scanning image of aluminum foam and establish an FEM model, as shown in Fig. 1.

Since there is a great difference between the matrix and holes in the gray-scale, the threshold segmentation is used to separate the matrix from the image in binarization processing. Here, the determination of the threshold is most important. There are several methods to determine the threshold, such as histogram troughs law, OTSU segmentation method (OTSO stands for Nobuyuki Otsu), and maximum entropy method, and so on. The maximum entropy was firstly

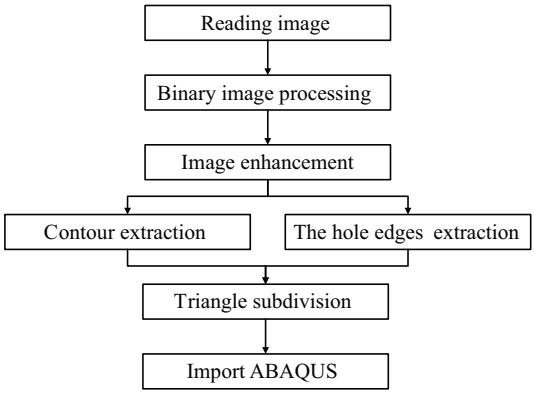

Fig. 1. FE modeling process based on MATLAB image processing.

proposed by Pun[22] which is adopted in this work. The purpose was to divide the gray-level histogram of image into separate classes and to make maximum total entropy of all kinds of classes.

S in this paper denotes a gray level and potential segmentation threshold point, $p_0, p_1, p_2, \ldots, p_L$, is the probability distribution of gray levels, then it is divided into two probability distributions at the gray level S. A represents the foreground and B represents the background,

$$A : \frac{p_0}{p_d}, \frac{p_1}{p_d}, \frac{p_2}{p_d}, \ldots, \frac{p_S}{p_d}, \quad B : \frac{p_{S+1}}{1-p_d}, \frac{p_{S+2}}{1-p_d}, \ldots, \frac{p_L}{1-p_d}, \tag{1}$$

where $p_d = \sum_{i=0}^{S} p_i$, L is the number of gray levels. Then, the entropy after segmentation image is calculated as follows

$$H(S) = E_A + E_B, \quad E_A = -\sum_{i=0}^{S} \frac{p_i}{p_d} \lg\left(\frac{p_i}{p_d}\right), \quad E_B = -\sum_{i=S+1}^{L} \frac{p_i}{1-p_d} \lg\left(\frac{p_i}{1-p_d}\right). \tag{2}$$

When the entropy of image, H_0, has a maximum, the best threshold value of image segmentation is given as $H_0 = \arg\max_S(H(S))$.

If the exponential entropy, H_N, is adopted, the entropy after segmentation image can be obtained from Eq. (2) as

$$H_N(S) = \sum_{i=0}^{S} \frac{p_i}{p_d} \exp\left(1 - \frac{p_i}{p_d}\right) + \sum_{i=S+1}^{L} \frac{p_i}{1-p_d} \exp\left(1 - \frac{p_i}{1-p_d}\right). \tag{3}$$

Then the optimal threshold value of divided images is given as $H_0 = \arg\max_S(H_N(S))$.

Image enhancement is an operation to remove noise and highlight useful information. For the μCT scanning image of aluminum foam, the noise is mainly caused by the basic properties of light and electricity, and it may be enhanced after image binarization processing, characterized by the "salt & pepper" noise. For this type of noise, the median filtering algorithm is very effective.

The extraction of external contour and internal boundary is an important step to reconstruct

the geometric model of aluminum foams. The image edge detection is usually done by the first order or second order derivative. The common edge detection operator in MATLAB is Robert gradient operator, Sobel operator, Prewitt operator, Laplacian, and so on. For aluminum foams, the "edge" function, provided by the MATLAB, is applied to detect the boundaries of aluminum foam matrix through constructing Prewitt operator, as shown in Fig. 2.

In the process of FE analysis, the mesh quality has a critical influence on the calculation results. In order to obtain effective calculation results based on porous structures of aluminum foam, more efficient meshing algorithm is needed. In this paper, the triangulation method is applied to mesh the aluminum foam directly. However there are many holes inside the aluminum foam and their distribution is random, which brings some difficulties to Delaunary triangulation. Two-step node filtration method is used to mesh this geometric model with island features. First of all, the global geometric model is meshed by Delaunary triangulation. Secondly, point-by-point filtering method is used to delete the triangular mesh with 4 internal boundary points, and the element is re-numbered. The result of two-step node filtration method is shown in Fig. 3. It is worth noting that the pixels on the boundary must be chosen as the node, and the interval take point method is used to pick up the node of matrix in the premise of guaranteeing minimal difference between the geometric model and the real one.

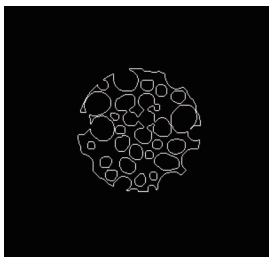

Fig. 2. Extraction of external contour and internal boundary.

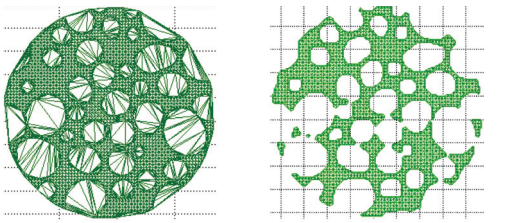

(a) global subdivision (b) subdivision with constraint

Fig. 3. Delaunary triangle subdivision of aluminum foam materials.

In conclusion, FEM is established by using the direct method, selecting node from all of pixels directly, and then meshing the structure. In this way, there is a smaller difference in structure size between the geometric model and the real one, and accordingly a lot of computer resources can be saved and the computational efficiency can be improved by controlling the number of the nodes on the premise of guaranteed authenticity.

The compression behavior at 25°C, 100°C, 200°C are measured on the INSTRON 5567 testing system under the displacement control with a loading speed of 1 mm/min, and the experiment results are shown in Figs. 4 and 5. Here, diameter and height of the aluminum foam are 70 mm and 35 mm, respectively.

As is known, the compression of aluminum foam material is divided into three stages: linear elastic stage, plastic platform stage, and densification stage. When the deformation is small, the load and displacement relation is linear, and the stage is very short which mainly reflects the strength characteristics of the pore structure. Then a longer plastic yielding platform appears with increasing compressive deformation. But the load almost remains the same as the deformation increases, and this stage mainly reflects the fact that the walls of the pores are crushed. Finally,

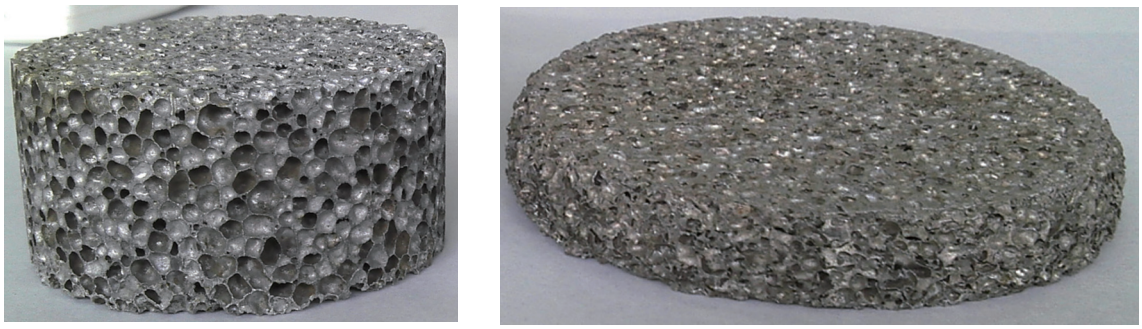

(a) before compression (b) after compression

Fig. 4. Comparing results before and after compression of aluminum foam.

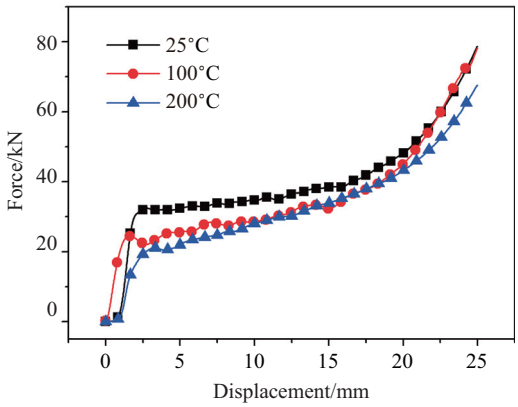

Fig. 5. Force–displacement curves at 25°C, 100°C, 200°C.

all holes are crushed, and the walls of the pores squeeze together. In this stage, the aluminum foam material is compacted (as shown in Fig. 4(b)), and the load increases rapidly. As shown in Fig. 5, the experiment curves have three stages and the yield stress is decreased with increasing test temperature, which is equal to 90 MPa, 63 MPa, and 58 MPa, respectively.

The μCT testing system is employed to scan the aluminum foam as shown in Fig. 4(a). The μCT employed in this study consists of a 40–60 keV X-ray power, with initial current of 100–180 μA, and a standard camera which has three levels viz: Standard (250 projections per slice); Medium (500 projections per slice); High (1000 projections per slice). 40 keV, 100 μA initial current, medium resolution option was adopted in this study. The μCT scanning images are shown in Fig. 6. To reduce the rather large amount of data in reconstructing the full-size model, a smaller size is selected to rebuild the geometrical model, of which the diameter and height are 14 mm and 8 mm, respectively. The sampling location is shown in Fig. 6. A novel 3D reconstruction method based on MATLAB is used to rebuild the FEM model of aluminum foam. The maximum entropy algorithm is employed to obtain the binarization image, as shown in Fig. 7. The median filtering algorithm is used to reduce the "salt & pepper" noise after binarization. The external contour and internal pore boundary is extracted by the "edge" function in MATLAB, and then a geometrical model is reconstructed, as shown in Fig. 8. Figure 9 shows a two-step mesh

algorithm is used to mesh the reconstructed geometrical model.

The boundary condition of aluminum foam compression FEM is shown in Fig. 10. The indenter is a rigid body, contacting with the upper surface of the specimen in the process of trial. The frictionless contact boundary condition is used. The bottom surface of the specimen is under displacement constraint, and the related condition is shown in Fig. 10. Here, the element type is chosen as C3D4H, and the martial is ZL102. The Young's modulus at 25°C, 100°C, 200°C are 25 GPa, 17 GPa, 11 GPa, respectively, and the Poisson ratio is 0.33. The real stress–strain curves at 25°C, 100°C, 200°C are shown in Fig. 11.

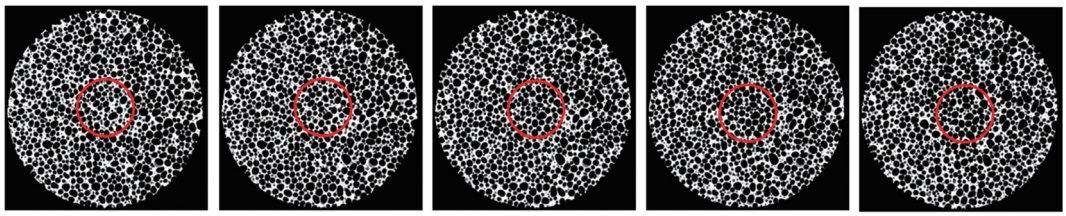

(a) 0 mm (b) 2 mm (c) 4 mm (d) 6 mm (e) 8 mm

Fig. 6. μCT scanning image.

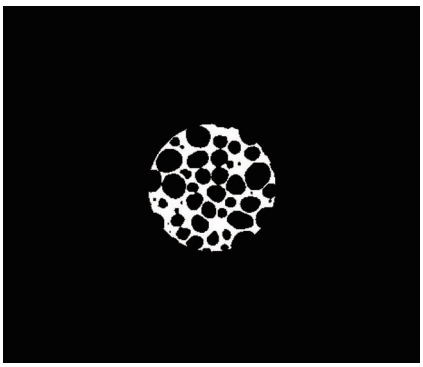

Fig. 7. Binary image.

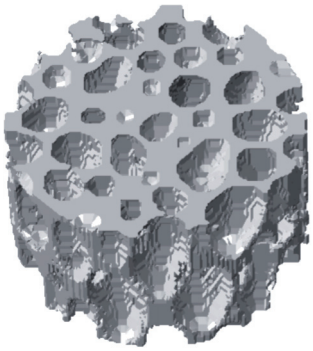

Fig. 8. Reconstruction geometrical model.

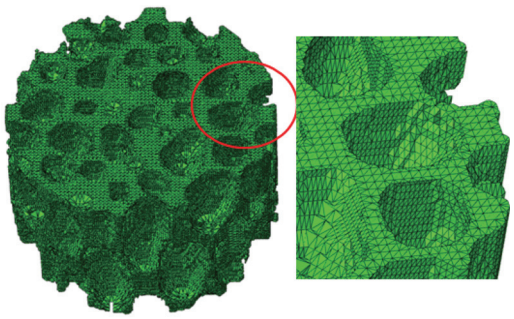

Fig. 9. Mesh of the reconstructive geometrical model.

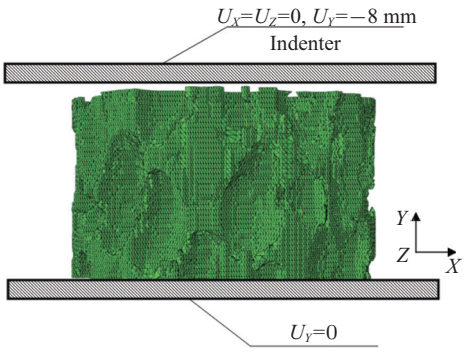

Fig. 10. Compression FEM and boundary condition of aluminum foam materials.

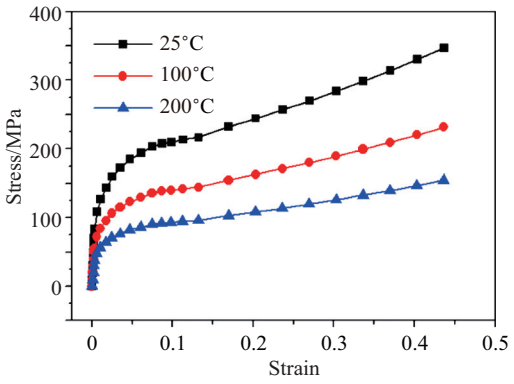

Fig. 11. Stress–strain curves at 25°C, 100°C, 200°C.

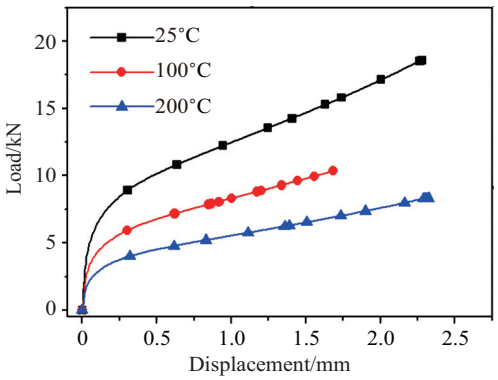

Fig. 12. Load–displacement curves at 25°C, 100°C, 200°C.

The FE calculation results of the aluminum foam at 25°C, 100°C, 200°C are shown in Fig. 12. The calculation yield stresses at 25°C, 100°C, 200°C are 95.273 MPa, 68.75 MPa, 64.41 MPa, respectively. The errors are 5.86%, 9.13%, and 11% comparing with the experiment results. According to some statistics, the porosity of the original sample is 58%, but the porosity of the small sample (14 mm diameter and 8 mm height) is 51.5%, which is the main error-source. From the numerical examples, it can be found that the calculation results agree with the experiment with maximum error less than 15%, which proves that the reconstruction geometrical method proposed in this work is applicable.

The stress distributions at 25°C are shown in Fig. 13 for different compression displacement. It shows that the Mises stress equals to 0 at the beginning of compression. The stress is gradually reaching the yield stress of matrix material with increasing compression displacement, then the aluminum foam begins to deform plastically. When the aluminum foam begins to deform plastically, the stress is nearly constant, and the aluminum enters into the second stage of compression deformation.

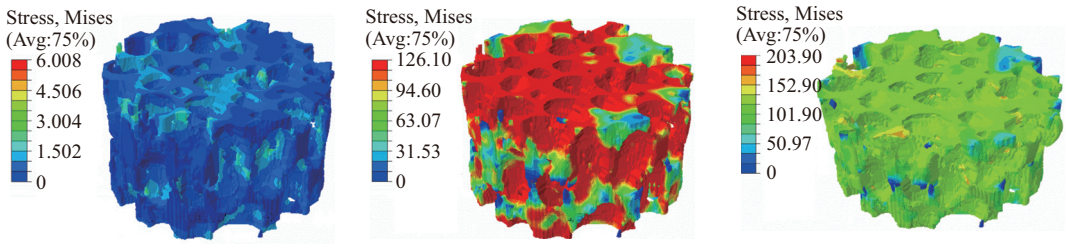

(a) (b) (c)

Fig. 13. Stress distribution at 25°C in different compression displacement.

In this work, a novel modeling method of cellular materials is proposed based on MATLAB image processing and synchrotron X-ray computed tomography scanning, and accordingly an FEM of aluminum foam is built. Maximum calculation error of the yield stress of aluminum foam is 11% compared with the experimental results, and the calculation of aluminum foam can describe mechanical behavior in the compression process, and the good numerical results show

that the present method is applicable. The compression experiment curves of aluminum have three stages and the yield stress decreases with the increase of test temperature.

This work was supported by the National Natural Science Foundations of China (11202007, 11232001, and 91216301).

1. H. Bafti, A. Habibolahzadeh. Compressive properties of aluminum foam produced by powde-Carbamide spacer route. *Materials and Design* **52**, 404–411 (2013).
2. J. U. Cho, S. J. Hong, S. K. Lee, et al. Impact fracture behavior at the material of aluminum foam. *Materials Science and Engineering A* **539**, 250–258 (2012).
3. P. D. Jaeger, C. T. Joen, H. Huisseune, et al. Assessing the influence of four bonding methods on the thermal contact resistance of open-cell aluminum foam. *International Journal of Heat and Mass Transfer* **55**, 6200–6210 (2012).
4. P. D. Jaeger, C. T. Joen, H. Huisseune, et al. Assessing the influence of four cutting methods on the thermal contact resistance of open-cell aluminum foam. *International Journal of Heat and Mass Transfer* **55**, 6142–6151 (2012).
5. R. B. Zhang, G. Q. Chen, W. B. Han. Synthesis, mechanical and physical properties of bulk Zr2Al4C5ceramic. *Materials Chemistry and Physics* **119**, 261–265 (2010).
6. A. N. Gent, A. G. Thomas. The deformation of foamed elastic materials. *Journal of Applied Polymer Science* **1**, 107–113 (1959).
7. A. N. Gent, A. G. Thomas. Mechanics of foamed elastic materials. *Rubber Chemistry Technology* **36**, 597–610 (1963).
8. L. J. Gibson, M. F. Ashby. Cellular Solids: Structures and Properties. Cambridge University Press, Cambridge (1997)
9. W. E. Warren, A. M. Kraynik. The linear elastic properties of open-cell foams. *Journal of Applied Mechanics* **55**, 341–346 (1988).
10. W. E. Warren, A. M. Kraynik. Linear elastic behavior of a low-density Kelvin foam with open cells. *Journal of Applied Mechanics* **64**, 787–794 (1997).
11. M. W. D. van der Burg, V. Shulmeister, E. van der Giessen, et al. On the linear elastic properties of regular and random open-cell foam models. *Journal of Cellular Plastics* **33**, 31–54 (1997).
12. N. Chawla, R. S. Sidhu, V. V. Ganesh. Three-dimensional visualization and microstructure-based modeling of deformation in particle-reinforced composites. *Acta Materialia* **54**, 1541–1548 (2006).
13. L. L. Michnaevsky. Automatic voxel-based generation of 3D micro structural FE models and its application to damage analysis of composites. *Materials Science and Engineering A* **407**, 11–23 (2005).
14. Z. Shan, A. M. Gokhale. Micromechanics of complex three-dimensional microstructures. *Acta Materialia* **49**, 2001–2015 (2001).
15. A. Sreeranganathan, S. I. Lieberman, H. Singh, et al. Realistic micromechanical modeling and simulation of boron modified titanium alloys. Proceedings of 2007 ABAQUS Users' Conference. Paris, 546–558 (2007).
16. J. Bock, A. M. Jacobi. Geometric classification of open-cell metal foams using X-ray micro-computed tomography. *Materials Characterization* **75**, 35–43 (2013).
17. N. Michailidis, F. Stergioudi, H. Omar, et al. An image-based reconstruction of the 3D geometry of an Al open-cell foam and FEM modeling of the material response. *Mechanics and Materials* **42**, 142–147 (2010).
18. T. Guillén, Q. H. Zhang, G. Tozzi, et al. Compressive behavior of bovine cancellous bone and bone analogous materials, microCT characterization and FE analysis. *Journal of the Mechanical Behavior of Biomedical Materials* **4**, 1452–1461 (2011).
19. N. Michailidis, F. Stergioudi, H. Omar, et al. Experimental and FEM analysis of the material response of porous metals imposed to mechanical loading. *Colloids and Surface A: Physicochemical and Engineering Aspects* **382**, 124–131 (2011).
20. G. Fischer, J. Nellesen, N. B. Anar, et al. 3D analysis of micro-deformation in VHCF-loaded nodular cast iron by μCT. *Materials Science and Engineering A* **577**, 202–209 (2013).
21. J. J. Williams, J. Segurado, J. Lorca, et al. Three dimensional (3D) microstructure-based modeling of interfacial decohesion in particle reinforced metal matrix composites. *Materials Science and Engineering A* **557**, 113–118 (2012).
22. T. Pun. A new method for gray-level picture thresholding using the entropy of the histogram. *Signal Processing* **2**, 223–237 (1980).